Ablation of Galileo Probe Heat-Shield Models in a Ballistic Range

Chul Park*
NASA Ames Research Center, Moffett Field, California
and
A. Balakrishnan*
PEDA Corporation, Palo Alto, California

Several 1/24-scale models of the Galileo Probe made of carbon-phenolic materials were flown in a ballistic range to test their ablation characteristics. Mostly radiative or all-convective heating environments were produced by using argon or air as the test gas, respectively, to simulate the Jovian entry heating environments. The experimental results were compared with the theoretical predictions made using the computer codes of radiating shock layer environment (RASLE) and charring materials ablation (CMA). The experimental data obtained in argon agreed approximately with the theoretical predictions. The data for air agreed approximately with the theory when turbulence and surface roughness effects were accounted for. The data imply that the Galileo Probe heat shield was adequately designed.

Nomenclature

C_f = skin friction coefficient
h = roughness dimension, cm
$\dot{m}$ = ablation rate, g/(cm^2-s)
p_∞ = freestream pressure, Torr
q = wall heat-transfer rate, kW/cm^2
R = nose radius, cm
Re = $\rho_\infty V_\infty R/\mu_\infty$
s = streamwise distance along the wall, cm
U_e = tangential velocity, cm/s
V_∞ = freestream velocity, km/s
δ = surface recession, mm
ρ = density
μ = viscosity

Subscripts

A = radiation from inviscid shock layer
c = convective
e = edge of shock layer
F = Fay and Riddell
p = peak value
r = radiative
s = steady state, smooth wall
t = transient, smooth wall
T = transient, rough wall
0 = stagnation point
∞ = freestream

Introduction

IN May 1986, an unmanned spacecraft named Galileo is scheduled to be launched, destined for the planet Jupiter. The Galileo spacecraft consists of two vehicles: the Orbiter and the Probe. The Probe will be separated from the Orbiter prior to arrival at Jupiter, and will enter the atmosphere of the plant. The vehicle is protected from the intense heat (mostly radiation from the hot shock layer) during the entry flight by a heat shield made of carbon-phenolic material. The heat shield is a sphere-cone with a cone half angle of approximately 45 deg. The spherical-nose region of the heat shield is made of chop-molded carbon-phenolic material, and the conical-frustum region is made of a tape-wrapped carbon-phenolic material.[1-3]

The heating environments and the expected ablation behavior of the heat shield have been studied to a great extent, both theoretically and experimentally. Several computer codes have been developed to numerically simulate the ablation phenomenon.[4] These computer codes assume a smooth wall, account for the turbulence produced by the flow shear, and were found to yield approximately the same ablation rates, provided the same physcial constants are used.[4] The most important unknown among these physical constants is the so-called "heat of ablation," which is defined as the ratio of the wall heat-transfer rates to the ablation rates and is associated with the heats of formation of the various ablation product gas species present in the boundary layer. The Galileo Probe heat shield was designed with a set of thermodynamic parameters corresponding to a heat of ablation of 22 MJ/kg, with a 30% to 50% overall safety margin.[2,3]

To date, three different types of ablation experiments supporting the Galileo Probe heat-shield design have been reported, i.e., laser irradiation tests,[5,6] ballistic-range tests of flat disks,[7,8] and arc-jet tests.[9] These tests pertain to the ablation behaviors in the stagnation region, which is dominated by radiation and is insensitive to fluid mechanical phenomena, such as turbulence. The three types of experiments complemented and their results agreed with each other, showing that the overall ablation rates (including possible spallation) are lower than assumed in the design of the heat shield by nearly 25% at the low heating rates, and approach the design values at high heating rates. In terms of the heat of ablation, the ablation (including spallation) were close to those corresponding to 30 MJ/kg at low heating rates, and approached those corresponding to 22 MJ/kg at high heating rates.

The present work is a part of the overall effort just described, and addresses the ablation characteristics mainly in the conical-frustum region, where shear is present and turbulence is important. In the present work, scale models of the Galileo Probe heat shield made of the chop-molded carbon-phenolic material and a carbon-phenolic material resembling the tape-wrapped carbon-phenolic material used in the

Received Oct. 4, 1983; revision received March 26, 1984. This paper is declared a work of the U.S. Government and therefore is in the public domain.

*Research Scientist. Member AIAA.

Galileo Probe were flown in a ballistic range filled with either argon or air. In argon, the shock-layer temperatures and radiative heat fluxes were similar to those in the Jovian flight. In air, heating resulted from convection and chemical generation, which are sensitive to turbulence and wall roughness. The characteristic Reynolds numbers of these experiments were nearly the same as those in the Jovian flight case.

The experimental results are compared with the theoretical predictions made using both Radiating Shock Layer Environment[10] (RASLE), one of the several environmental codes employed during the design of the Galileo Probe heat shield, and Charring Materials Ablation[11] (CMA), the materials-response code employed in the design. The RASLE code assumes, as do other similar codes, a smooth wall. To the degree of precision expected in this study, the theoretical values agreed with the experimental results when the wall roughness effect was accounted for. The present study leads to the conclusion that the Galileo Probe heat shield is adequately designed for the conical-frustum region.

Experiment

General Description

A total of eight models made of carbon-phenolic materials were successfully launched and recovered in the track-range facility of the G-range of Arnold Engineering Development Center, Arnold Air Force Station, Tenn.[12] The models were made in the shape of a sphere-cone with a conical half angle of 45 deg. The nose and overall (i.e., frustum edge) radius of the models were 1.27 and 2.54 cm, respectively. The dimensions chosen were approximately a 1/24 scale of the Galileo Probe.

Two types of carbon-phenolic materials were tested: a 20-deg inverted-chevron carbon-phenolic (ICCP) made of type FM 5055A prepreg, and a chop-molded carbon-phenolic (CMCP) made of FM 5055G prepreg. The two types of fibers are known to have nearly identical thermochemical properties.[7-9] The CMCP is the same material as that used in the nose region of the Galileo Probe. The ICCP is similar to the tape-wrapped carbon-phenolic material used over the conical region of the Galileo Probe; because of the difference in scales, the tape-wrapped carbon-phenolic material was not appropriate for the present experiment.

Two different model designs were employed, as sketched in Fig. 1. The ICCP models were machined into the shape of a cap, and glued on the aluminum substrate. The CMCP models were made into the shape of a cork, and were glued on an aluminum boss. Further details of the model design are given in Refs. 13 and 14. The 20-deg conical half angle of the cloth ply in the ICCP models was facing inward into the flow, as illustrated in Fig. 1, and the spacing between the adjacent layers of the cloth was approximately 0.5 mm. For the CMCP models, the 1.2-cm^2 cloth coupons were placed in the plane normal to the axis of the model.

Argon and air were used as the test gases. Argon was used in order to subject the models to radiative heating.[15] The range has two sections: the "uprange," 93 m in length; and the "downrange," 174 m in length. In two of the eight shots made (shots 5595 and 5603), both sections were filled with argon. For another two shots (shots 5474 and 5477), both were filled with air. For the remaining shots, the uprange was filled with argon and the downrange was filled with air. Pressures in the two sections were kept at the same levels, and were in the range of 75-300 Torr.

The records of velocity and travel distance as compared with travel time are given in Refs. 16 and 17. The velocity records are also shown in Fig. 2. Table 1 highlights the test environments and compares them with a typical Jovian entry flight condition. The quantity q_A, taken from Ref. 15, is the radiative heat flux emanating from the inviscid region of the shock layer and falling on the edge of the boundary layer at the stagnation point. The quantity q_F is the convective heat-transfer rate given by the formula of Ray and Riddell[18] at zero mass injection. Table 1 shows that the present experiment approximately reproduced the Reynolds numbers and the heat fluxes (q_A and q_F) predicted for the Jovian flight.

Recession Measurement

Surface recessions were measured on each model after recovery from the range. For the ICCP models, the recession measurements was carried out in three different ways: contouring, x-ray, and sectioning. In the contouring method, a template representing the original contour in the models was brought adjacent to the model, as shown in Fig 3. The template was positioned in reference to the frustum edge. The gap between the template and the model contour was judged to be the surface recession. In the x-ray method, an x-ray photograph was taken of the profile of the models, as shown in Fig. 4. The thickness of the carbon-phenolic cap seen on the photograph was then compared with the original thickness to determine the difference. In the sectioning method, the models were sectioned into two halves, and the thickness of the carbon-phenolic cap was measured directly. For the

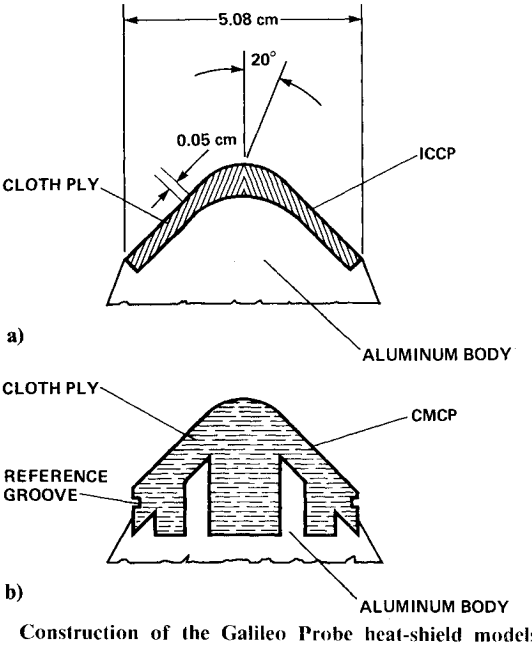

Fig. 1 Construction of the Galileo Probe heat-shield models: a) ICCP model, b) CMCP model.

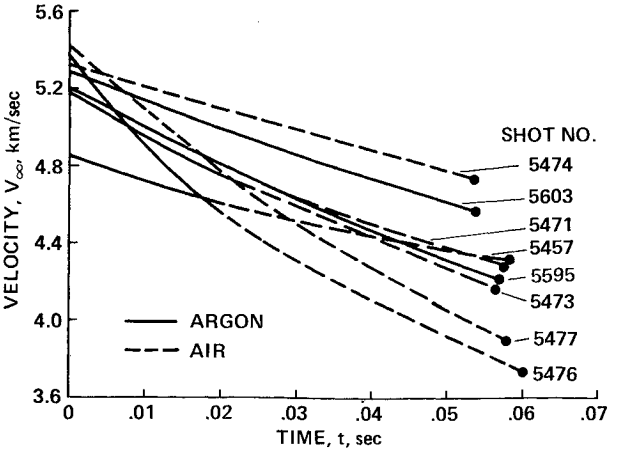

Fig. 2 Records of velocity vs time of test-model flights in the ballistic range.

CMCP models, only the contouring method was used. A template, made separately for the two CMCP models, was fitted to the model with the groove on the model as the reference. This technique is described in detail in Ref. 8.

Figure 5 shows the cross section of one of the CMCP models (shot 5595) after the test. The picture shows a relatively well-defined demarcation between the char layer and the virgin material. The char thickness was determined to be approximately 0.38 mm on the average for the case shown. For the two CMCP models, the char thickness was found to be nearly identical. For the ICCP models, the char layer was found to be thinner by about 12%. These char thicknesses are about 15% smaller than the thicknesses in the cases reported in Ref. 8. In Ref. 8, the swell of the char was determined to be about 0.06 mm. Since the swell is expected to be approximately proportional to char thickness, the swell thickness for the present test conditions was estimated to be about 0.05 mm. The swell was added to the measured recession to determine the overall recession value.

The stagnation-point surface recessions determined by the three methods just described are plotted in Fig. 6. The abscissa in the figure represents the computed steady-state recession, which will be described later. As the figures shows, the surface recessions as determined by the three methods agree fairly well. The averages of the three methods, shown as solid circles, represent the measured values to within ±12%.

In Figs. 7a-h, the measured recessions over the model surfaces are shown as solid curves. The abscissas in the figures are the normalized streamwise distance, i.e., the ratio of the streamwise distance measured from the stagnation point along the wall s to the nose radius R. The recessions shown here were obtained using the contouring method. The two different curves represent two sides of the stagnation point, i.e., left and right. As the figures show, the six ICCP models (shots 5457, 5471, 5473, 5474, 5476, and 5477) had considerable roughness; the amplitudes of the roughness exceeded 0.2 mm. Moreover, the surface coordinate fluctuation had an approximately constant interval of 0.5 mm, corresponding to the cloth ply spacing of the material. In comparison, the two CMCP models (shots 5595 to 5603) had smaller roughness (of the order of 0.1 mm or less) and no clear periodicity. In the figures, the dashed, chain, and double-chain curves are the theoretical values, which will be explained later.

Theoretical Interpretation

RASLE Calculations

To interpret the experimental recession data shown in Figs. 7a-h, a theoretical calculation was made using the computer code RASLE.[10] The radiative and thermochemical argon data necessary for the calculation were taken from Refs. 7 and 15. The radiative data for ablation product species include those of the absorption by C_3 in the far ultraviolet wavelength range.[19,20] The thermochemical properties for C_2H, C_3H, and C_4H used in the present calculation lead to an ablation energy value of approximately 30 MJ/kg, as opposed to the 22-MJ/kg value used in the design of Galileo Probe heat shield.[7,9,21]

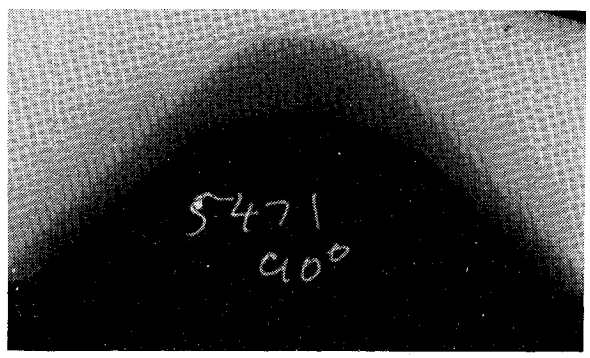

Fig. 4 x-ray photographs of the post-test model, shot 5471.

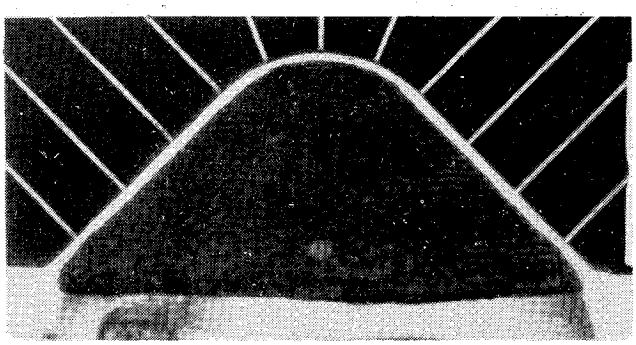

Fig. 3 Post-test model contour in relation to pretest contour represented by a template, shot 5471.

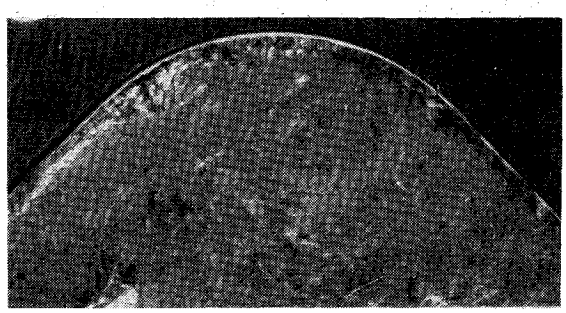

Fig. 5 Cross section of the post-test model in the stagnation region, shot 5595. The template represents the pretest contour.

Table 1 Test conditions of ballistic range experiments with carbon-phenolic models

Shot No.	Model		Test gas		Range pressure, Torr	Muzzle velocity, km/s	Stagnation pressure, atm		Uprange midpoint		
	Material	Design	Uprange	Downrange			Beginning	End	Re, 10^{-6}	q_A, kW/cm^2	q_F, kW/cm^2
Jovian[a]	—	—	—	—	3.2[b]	40.87	5.85	—	0.693[b]	59.0	13.7
5457	ICCP	Cap	Argon	Air	100	4.831	49.2	28.2	0.573	21.1	1.92
5471	ICCP	Cap	Argon	Air	150	5.188	85.0	42.6	0.910	61.5	3.33
5473	ICCP	Cap	Argon	Air	200	5.410	123.3	53.2	1.25	108.5	4.56
5474	ICCP	Cap	Air	Air	100	5.322	43.1	34.7	0.487	0	12.1
5476	ICCP	Cap	Argon	Air	300	5.371	182.2	65.0	1.82	143.0	4.10
5477	ICCP	Cap	Air	Air	300	5.432	134.6	107.1	1.44	0	20.36
5595	CMCP	Cork	Argon	Argon	100	5.203	57.0	38.1	0.611	36.6	3.09
5603	CMCP	Cork	Argon	Argon	75	5.297	44.3	33.4	0.472	33.4	3.38

[a] Predicted Jovian entry flight conditions taken from Refs. 2 and 3. [b] For an assumed temperature of 298 K.

A total of six solutions were obtained for argon under the assumption of a steady-state ablation. The calculated cases are summarized in Table 2, and are compared with the Jovian flight case. The turbulent solutions in the table (cases 1, 3, 5, and 6) were obtained by assuming that turbulence is triggered at the first computed station away from the stagnation point. The transition case for argon (case 4) was obtained by gradually increasing turbulence intensity from the stagnation point to the point $s/R=0.4$.

Figure 8 shows the wall heat-transfer rates obtained from one of the argon solutions, case 3, and compares them with those for the Jovian flight case. As seen here, the heat-transfer rates for the present test conditions are similar in magnitude to those of the Jovian flight case. In the range $0.15<s/R<0.55$, the convective component in the argon solution becomes negative. This is a result of the negative enthalpy gradient at the wall, produced by the fact that the freestream enthalpy of argon is less than the energy of ablation of the carbon-phenolic material, and occurs only under a high-radiative heating environment. Its magnitude is quite small compared with the radiative component.

In Fig. 9, the calculated ablation rates $\dot{m}$ for the six argon cases are normalized by the respective peak values $\dot{m}_p$ and are superposed on the same plot. As seen here, all four turbulent cases and the transitional case show nearly identical variation in $\dot{m}/\dot{m}_p$. These curves can be represented approximated by

$$\dot{m}/\dot{m}_p=\cos^2(s/R) \quad \text{for } s/R<0.8$$
$$=\cos^2(0.8) \quad \text{for } s/R>0.8 \tag{1}$$

and agree with the computed values to within $\pm 8\%$. The peak ablation rate $\dot{m}_p$ can in turn be expressed as

$$\dot{m}_p=1.057(p_\infty/100)(V_\infty/5)^{5.132}\,\text{g/(cm}^2\text{-s)} \tag{2}$$

where p_∞ is the freestream pressure in Torr and V_∞ is the flight velocity in km/s, to within an accuracy of 3%. By combining Eqs. (1) and (2), the theoretical ablation rates over the models are completely specified for the steady-state turbulent condition in argon.

In the cases where the test gas is air, radiation is negligibly weak and hence was ignored in the calculation. A total of 10 solutions were obtained for air, as indicated in Table 2. As for argon cases, the turbulent air solutions were obtained by assuming that turbulence is triggered immediately downstream of the stagnation point. The transitional case, case 9, was obtained by triggering turbulence suddenly at $s/R=0.75$. This triggering point was selected in accordance with the findings of Reda,[22,23] which showed that transition over a smooth wall occurs approximately at this point for the flight environments similar to the present test environments.

In Fig. 10, the ablation rates are compared for $p_\infty=100$ Torr for a laminar case, a transitional case, and four turbulent cases normalized by the peak value for the turbulent cases. As seen here, there are large differences among the three cases. Since the walls of the test models were rough (see Figs. 7a-f), the fully turbulent solutions were chosen for comparison with the experimental data in the present work. In Fig. 11, all computed turbulent cases for air are superposed on a normalized scale. As seen here, the normalized profiles are nearly the same. Hence, the profiles are represented by a single curve, chosen arbitrarily as case 10 ($p_\infty=100$ Torr, $V_\infty=5.02$ km/s)

$$\dot{m}/\dot{m}_0=\text{the profile for case 10} \tag{3}$$

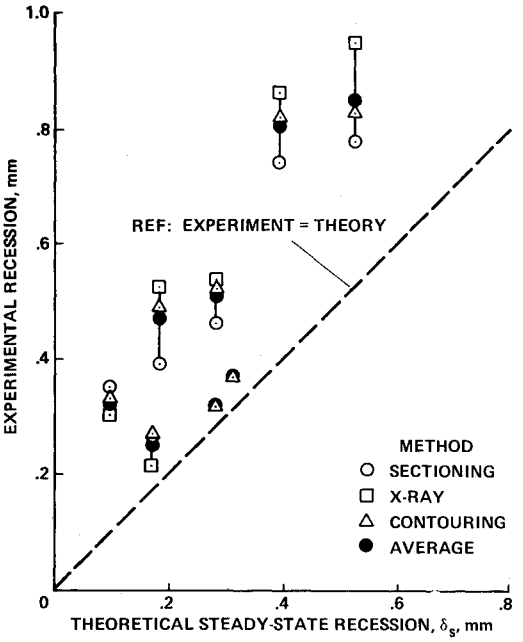

Fig. 6 Comparison of the stagnation-point recessions of the test models, determined by the three methods.

Table 2 Summary of RASLE solutions (steady state)

Case	Atmosphere	Freestream Pressure, Torr	Freestream Velocity, km/s	Laminar/ transition/ turbulent	Stagnation point Pressure, atm	Stagnation point Radiative q, kW/cm^2	Stagnation point Convective q, kW/cm^2	Ablation rate, g/cm^{2}s
Jovian[a]		3.2[b]	40.87	Turbulent	5.85	23.7	0.032	0.994
1	Argon	100	4.715	Turbulent	39.9	19.5	2.74	0.766
2			5.020	Laminar	45.9	31.3	2.15	1.05
3				Turbulent	45.9	31.3	2.15	1.05
4		150		Transition	68.6	54.8	2.11	1.65
5		200	4.715	Turbulent	79.3	45.5	6.20	1.59
6		200	5.020		91.2	69.2	3.69	2.21
7	Air	100	4.715		35.6	0	4.85	0.236
8			5.020	Laminar	40.4		5.65	0.275
9				Transition				
10				Turbulent				
11		150	4.715		47.0		4.21	0.296
12		150	5.020		53.4		5.26	0.354
13		200	4.715		62.6		5.02	0.351
14		200	5.020		71.1		6.22	0.407
15		300	4.715		93.8		6.50	0.449
16		300	5.020		106.6		7.98	0.518

[a] Predicted Jovian entry flight conditions taken from Refs. 2 and 3. [b] For an assumed temperature of 298 K.

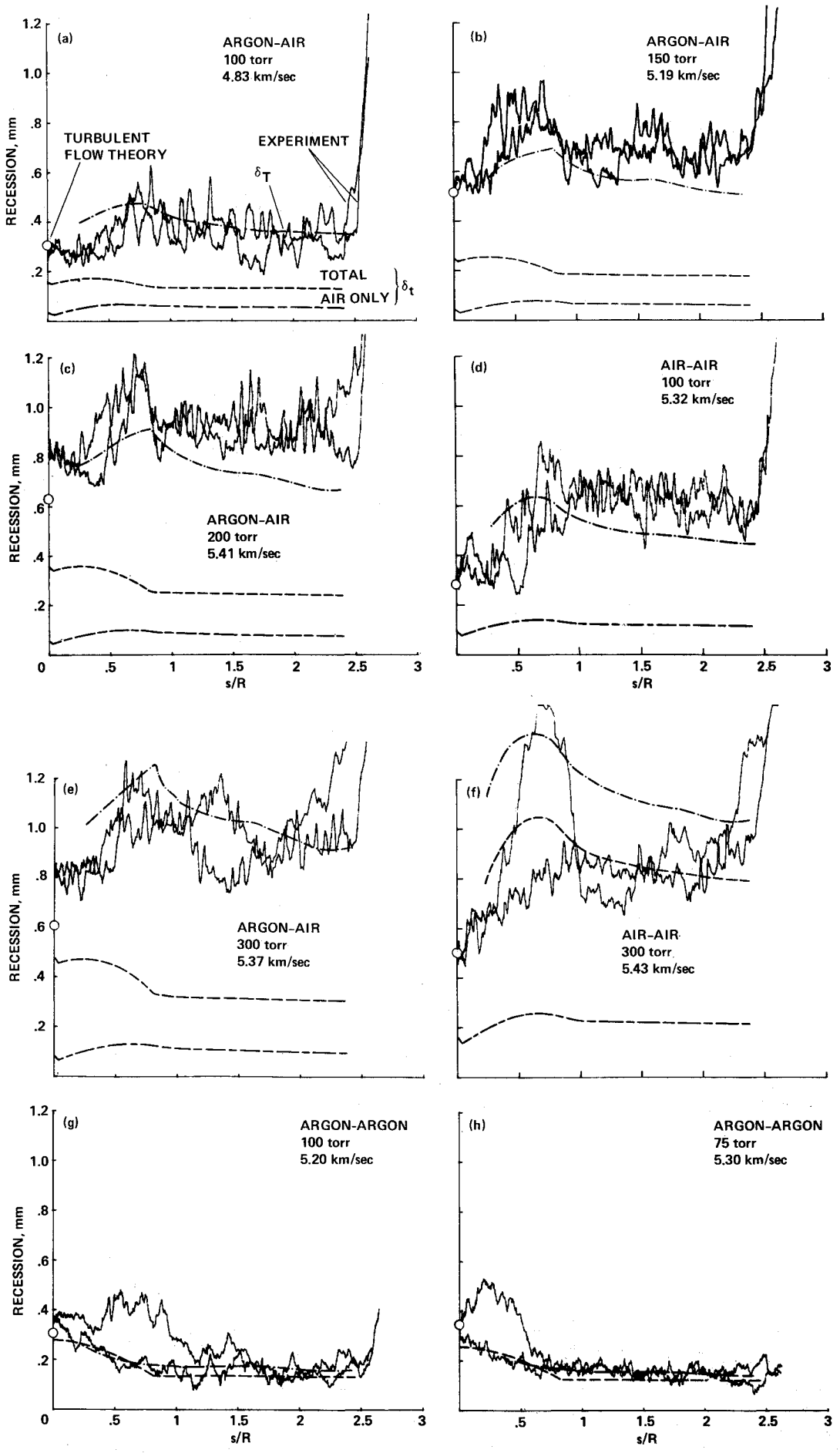

Fig. 7 Comparison of the calculated and measured surface recessions: a) shot 5457, b) shot 5471, c) shot 5473, d) shot 5474, e) shot 5476, f) shot 5477, g) shot 5595, and h) shot 5603.

where

$$\dot{m}_0 = 0.261(p_\infty/100)^{0.585}(V_\infty/5)^{1.161}(\text{g/cm}^2)\text{-s} \quad (4)$$

which represents the computed values to within ±5%. Equations (3) and (4) completely specify the computed steady-state turbulent ablation rates for air.

Time Integration

By integrating $\dot{m}$ in Eqs. (1-4) over time, and dividing the results by the density of the virgin material, one obtains the surface recessions corresponding to the steady-state ablation

$$\delta_s = \int \dot{m} \frac{dt}{\text{solid density}} \quad (5)$$

This quantity was used for the abscissa in Fig. 6. The steady-state ablation model ignores the transient heat conduction and pyrolysis phenomena in the solid, and, hence, tends to overestimate recession. To account for the two neglected phenomena, a transient ablation calculation was carried out using the computer code CMA.[11] The calculation was made only for the stagnation point where such a calculation is simple. The heat-transfer rates to the stagnation point under the transient condition are determined by the method described in Ref. 7. The results showed that surface recessions under the transient condition δ_t can be approximated by

$$\delta_t = 0.9\delta_s \quad (6)$$

to within ±3%. This relation is assumed to hold for the points away from the stagnation point as well. By limiting the integrating interval in Eq. (5) to either uprange or downrange, one can obtain the uprange or downrange contribution to δ_t.

In Figs. 7a-h, the δ_t values obtained by Eq. (6) are shown and are compared with the experimental data. For the cases where the uprange and downrange were filled with different gases, the contribution of one gas is also shown. The figures show that, except for shots 5595 and 5603, the calculated smooth wall recession δ_t was considerably underestimated.

Injection-Induced Turbulence at Stagnation Point

As mentioned earlier, the RASLE code assumes that the wall surfaces are perfectly smooth and that a laminar sublayer exists adjacent to the wall. For a laminar sublayer to exist under a strongly ablating condition, the ablation product gases must emanate from the wall in a perfectly laminar manner. However, strongly ablating surfaces are likely to produce turbulence at the wall,[24] and such injection-induced turbulence will eliminate a laminar sublayer.

For the stagnation point where the boundary-layer flow is believed to be laminar, Ref. 24 shows evidence that such injection-induced turbulence causes an increase in ablation rate when the ablation rate is large. Since the experimentally observed stagnation-point recessions were significantly larger than those predicted by RASLE in the present work, the calculation of Ref. 24 was carried out to verify the cause of this discrepancy. In the theory of Ref. 24, intensities of the injection-induced turbulence are characterized by a time constant representing the average period of temporal fluctuation in injection velocity. For graphite, carbon-carbon composites, and carbon-phenolic materials, Ref. 24 shows that the time constant lies between 0.0001 and 0.0003 s. The time constant was assumed to be 0.0002 s in the present calculation. The results are shown as circles in Figs. 7a-h. As seen in the figures, the turbulent stagnation-point values are closer to the experimental values. One can, therefore, attribute the observed disagreement between the experimental data and the RASLE predictions at the stagnation point to the injection-induced turbulence.

For shots 5595 and 5603, enhancement of ablation by injection-induced turbulence is small; the experimental recession values and the theoretical values accounting for the injection-induced turbulence are only slightly higher than those given by RASLE. This is because, for these two shots, radiation was the dominant heating mechanism at the stagnation point, as the models flew only in an argon environment. Injection-induced turbulence affects only the convective component of the heat-transfer rate for this case.

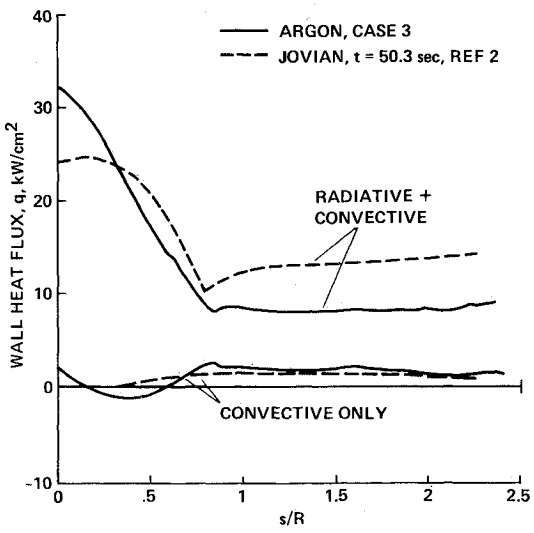

Fig. 8 Distribution of computed wall heat fluxes over the heat shield for a typical Jovian flight case and a present case.

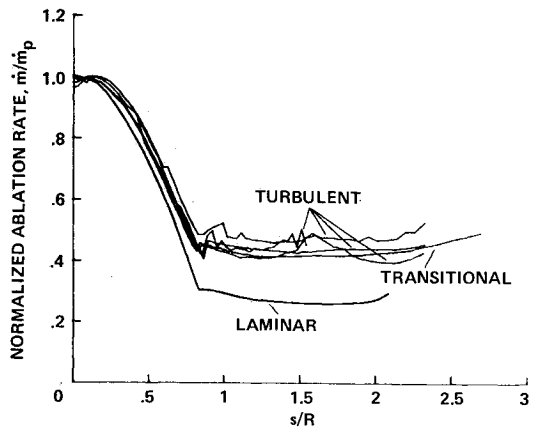

Fig. 9 Calculated ablation rate distribution, $\dot{m}/\dot{m}_p$, for argon.

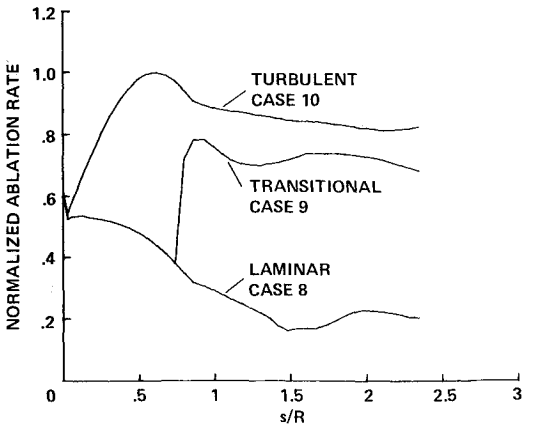

Fig. 10 Calculated ablation rates for air flows; $p_\infty = 100$ Torr, $V_\infty = 5.02$ km/s, normalized to $\dot{m}_p$ for case 10.

The difference between the results of these two shots and those of the other shots cannot be attributed to the difference in materials (CMCP vs ICCP): the two materials ablate at nearly the same rate under a mostly radiative environment.[7,8]

Surface Roughness

For the regions away from the stagnation point, it is not known at present how the injection-induced turbulence interacts with other sources of turbulence. Moreover, the models used in the present experiment had rough surfaces, which must have enhanced the wall heat-transfer rate as well. For the present situation where a strong ablation as coupled with surface roughness, there is no known method of calculating ablation rate reliably. In order to show a general trend and to present a reasonable explanation of what was observed experimentally, a crude theoretical model was developed.

According to the model, both the convective heat-transfer rate and mass-transfer rate were assumed to be proportional to the skin-friction coefficient. For argon, the assumption leads to the expression

$$\frac{\dot{m}(\text{rough})}{\dot{m}(\text{smooth})} = \frac{1+(q_c/q_r)\,C_f(\text{rough})/C_f(\text{smooth})}{1+q_c/q_r} \tag{7}$$

where q_c and q_r denote convective and radiative components of the heat-transfer rate, respectively. The ratio q_c/q_r was assumed to be the same for all cases as in case 3 in Table 1. For air, the corresponding relationship is

$$\frac{\dot{m}(\text{rough})}{\dot{m}(\text{smooth})} = \frac{C_f(\text{rough})}{C_f(\text{smooth})} \tag{8}$$

The skin-friction coefficient for a smooth wall, C_f(smooth), was calculated from the flat-plate formula for subsonic flow

$$C_f(\text{smooth}) = 0.0576(\rho_e U_e s/\mu_e)^{-0.5} \tag{9}$$

where ρ_e, U_e, and μ_e are, respectively, density, tangential velocity, and viscosity at the edge of the shock layer (i.e., behind the shock wave), determined from the Newtonian flow theory. The friction coefficient for rough-wall, C_f(rough), conditions was taken from the completely turbulent case for a flat plate in subsonic flow[25]

$$C_f(\text{rough}) = [2.87 + 1.58\log_{10}(s/h)]^{-2.5} \tag{10}$$

where h is the roughness dimension. For the CMCP models (shots 5595 and 5603), h was taken to be 0.01 cm, the approximate extent of the observed surface roughness (see Figs. 7g and h). For the ICCP models (shots 5457, 5471, 5473, 5474, 5476, and 5477), h was taken to be equal to the cloth ply spacing, i.e., $h=0.05$ cm. From the preceding expressions, the combined effect of injection-induced turbulence and wall roughness was represented by an equivalent roughness effect. The $\dot{m}$(rough) values in Eqs. (7) and (8) were substituted in place of $\dot{m}$ in Eqs. (1-4) to obtain the recessions for rough surfaces. The calculation was made for the region $s/R>0.2$. The resulting recessions, including the transient phenomena, were denoted by δ_T, i.e.,

$$\delta_T = 0.9\int \dot{m}(\text{rough})\,\frac{dt}{\text{solid density}} \tag{11}$$

The results of the calculation are shown in Figs. 7a-h and are compared with the experimental data. There is reasonable agreement between the calculated rough-wall recessions δ_T and the experimental data, considering the very approximate nature of the theoretical model. One sees from this that the combination of surface roughness and injection-induced turbulence can account for the discrepancy between the experimental data and the predictions made using the RASLE code.

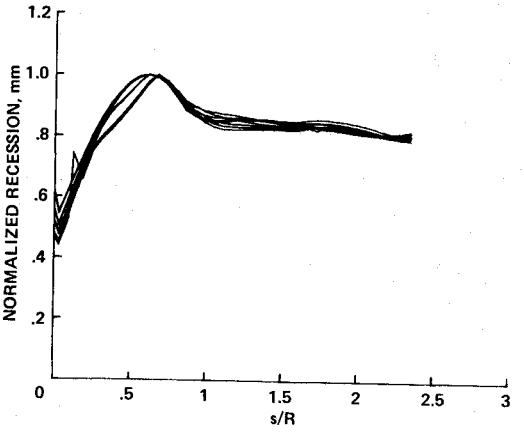

Fig. 11 Normalized ablation rates for turbulent flow in air; cases 7 and 10-16.

For shots 5595 and 5603 (Figs. 7g and h), the surface roughness effect is minor. Except for the regions $0.5<s/R<1.0$ in Fig. 7g and $0<s/R<0.5$ in Fig. 7h, which show anomalously large recessions, the three sets of recession values (the experimental value, the smooth-wall recession δ_T, and the rough-wall recession δ_T) are nearly the same. This is because, for the two shots, radiation was the main heating mechanism. The anomalously large recessions near the stagnation point are believed to result from the chipping of surface materials during the sectioning process.

Discussion

For shots 5595 and 5603 (Figs. 7g and h), which were flown in an argon-only atmosphere, and, hence, were subject mostly to radiative heating, RASLE calculation predicts the measured surface recessions reasonably closely, both at the stagnation point and over the frustum. Agreement is even closer if the injection-induced turbulence at the stagnation point and surface roughness are accounted for, although these effects are minor. The contribution of spallation, which is expected to be of the order of 10% for the two shots, is too small to be identified. Injection-induced turbulence and surface roughness have only minor influences on the two shots because they affect only convective heat- and mass-transfer phenomena. The good agreement between RASLE calculations and the experimental data validates the RASLE code, and by inference, other computer codes used in the design of the Galileo Probe heat shield. In the Jovian flight environment, radiation is expected to be even more dominant over convection than in the two shots (see Fig. 8). Hence, one expects an even closer agreement between the theory and experiment.

In an air environment, where heat transfer is purely convective, turbulence plays an important role. Even when the wall is smooth, turbulence can increase the ablation rate by a factor of 2 or 3 over a laminar flow in the conical region (see Fig. 10). At the stagnation point, where the boundary layer is believed to be laminar according to the classical theory, the injection-induced turbulence enhances the ablation rate significantly. Over the frustum region, the combination of injection-induced turbulence and surface roughness, which was represented in the present work by an equivalent surface roughness, increases the ablation rate by a factor of several. Here, the RASLE code is inadequate to predict surface recessions unless a due correction is made for the neglected effects.

In the Jovian entry flight, the convective contribution is important only during the last few seconds of the heating

period. The contribution of the convective period to the total recession is of the order of 10% (see Ref. 2). According to the present theoretical interpretation, ablation rates at the stagnation point will increase by a factor of about 2 during this period because of the injection-induced turbulence, leading to an overall recession enhancement of about 10%. The Galileo Probe heat shield has a safety margin of nearly 50% at the stagnation point,[2] so an enhancement of this magnitude easily can be tolerated.

Over the frustum, the present results can be extrapolated only if the relative contributions of injection-induced turbulence and surface roughness are known, and only after due consideration is given to the difference in body sizes between the Jovian entry case and the present experiment. The surface roughness effect is determined mostly by the ratio of roughness height to boundary-layer thickness. In the present theoretical model, the effect is represented by the ratio s/h in Eq. (10). In the Jovian flight case, the ratio s/h is about a factor of 20 larger than in the present experiment and, therefore, the surface recession due to roughness effects should be less in flight than that observed in the present tests. In fact, the enhanced recession due to roughness should not be more than a factor of two over the frustum region where the convective heating is important, provided the enhancement was due entirely to surface roughness. The Galileo Probe heat shield has a safety margin of about 30% over the frustum, and, hence, the enhancement of this magnitude can be tolerated. Contribution of injection-induced turbulence to the observed ablation enhancement over the frustum region is not known. If injection-induced turbulence is solely responsible for the observed ablation enhancement, one should expect nearly the same extent of ablation enhancement for the Galileo Probe. In this case, there will be an approximately 20% increase in the overall recession over the frustum region during the Jovian entry. The safety margin of 30% can still absorb this enhancement.

Conclusions

In the argon environments, where heating was mostly radiative and where heating rates and Reynolds numbers of the Jovian entry flight were closely simulated, surface recessions over the 1/24-scale models of the Galileo Probe heat shield agreed approximately with those predicted using RASLE and CMA codes, even though the pressure was higher. In the air environments, where the heating was all convective, the stagnation point recessions for the models were substantially higher than those predicted by RASLE, and agreed approximately with those calculated with the theory of injection-induced turbulence. Over the conical region of the models, the measured recessions were substantially higher than those predicted by RASLE, which could be attributed to the combination of injection-induced turbulence and surface roughness. The probable increases in surface recessions of the Galileo Probe heat shield resulting from these effects are within the margin of safety of its design thickness.

Acknowledgments

The authors wish to express their sincere thanks to A. M. Adams and his colleagues at Arnold Enginering Development Center, Arnold Air Force Station, Tenn., for fabricating the test models and carrying out the ballistic range experiment.

References

[1]Howe, J. T., Pitts, W. C., and Lundell, J. H., "Survey of the Supporting Research and Technology for Thermal Protection of the Galileo Probe," *Progress in Astronautics and Aeronautics, Thermophysics of Atmospheric Entry*, edted by T. E. Horton, Vol. 82, AIAA, New York, 1982, pp. 293-327.

[2]Green, M. J. and Davy, W. C., "Galileo Probe Forebody Thermal Protection," *Progress in Astronautics and Aeronautics, Thermophysics of Atmospheric Entry*, edited by T. H. Horton, Vol. 82, AIAA, New York, 1982, pp. 328-353.

[3]Balakrishnan, A. and Nicolet, W. E., "Galileo Probe Forebody Thermal Protection: Benchmark Heating Environment Calculations," AIAA Paper 81-1072, June 1981.

[4]Menees, G. P., "An Evaluation of Computer Codes for Simulating the Galileo Probe Aerothermal Entry Environment," AIAA Paper 81-1069, June 1981.

[5]Lundell, J. H. and Dickey, R. R., "Response of Heat-Shield Materials to Intense Laser Radiation," *Progress in Astronautics and Aeronautics, Outer Planet Entry Heating and Thermal Protection*, edited by R. Viskanta, Vol. 64, AIAA, New York, 1979, pp. 193-209.

[6]Lundell, J. H., "Spallation of the Galileo Probe Heat Shield," AIAA Paper 82-0852, Mo., June 1982.

[7]Park, C., "Stagnation-Point Ablation of Carbonaceous Flat Disks. Part 1. Theory," *AIAA Journal*, Vol. 21, Nov. 1983, pp. 1588-1594.

[8]Park, C., "Stagnation-Point Ablation of Carbonaceous Flat Disks. Part 2. Experiment," *AIAA Journal*, Vol. 21, Dec. 1983, pp. 1748-1754.

[9]Park, C., Lundell, J. H., Green, M. J., Winovich, W., and Covington, M. A., "Ablation of Carbonaceous Materials in a Hydrogen-Helium Arc-Jet Flow," AIAA Paper 83-1561, Montreal, Can., June 1983.

[10]Nicolet, W. E., "Radiation Heating Environments for Jovian Entry Conditions," *Progress in Astronautics and Aeronautics, Radiative Transfer and Thermal Control*, edited by A. M. Smith, Vol. 49, AIAA, New York, 1976, pp. 231-250.

[11]Kendall, R. M., Rindal, R. A., and Bartlett, E. P., "Thermochemical Ablation," AIAA Paper 65-642, Monterey, Calif., Sept. 1965.

[12]Norfleet, G. D., Hendrix, R. E., Raper, R. M., and Callons, E. E. Jr., "Development of an Aeroballistic Range Capability for Testig Re-entry Materials," *Journal of Spacecraft and Rockets*, Vol. 12, May 1975, pp. 302-307.

[13]Adams, A. M., "Hypervelocity Track Tests of the NASA Galileo Probe Heatshield," AEDC-TSR-80-V60, Arnold AFS, Tenn., Dec. 1980.

[14]Adams, A. M., "Hypervelocity Track Tests of the Ablation Characteristics of Heat Shield Materials for the NASA Galileo Probe," AEDC-TSR-80-V25, Arnold AFS, Tenn., Aug. 1981.

[15]Park, C., "Calculation of Radiation from Argon Shock Layers," *Journal of Quantitative Spectroscopy and Radiative Transfer*, Vol. 28, July 1982, pp. 29-40.

[16]Adams, A. M., "NASA/Ames Galileo Probe Heatshield Ablation Test, Data Package," Project No. V41 G-02, Arnold AFS, Tenn., Nov. 1980.

[17]Adams, A. M., "NASA/Ames Galileo Probe Heatshield Ablation Test 2, Data Package," Project No. C378-VG, Arnold AFS, Tenn., Aug. 1981.

[18]Fay, J. A. and Riddell, F. R., "Theory of Stagnation Point Heat Transfer in Dissociated Air," *Journal of the Aeronautical Sciences*, Vol. 25, Feb. 1958, pp. 73-97.

[19]Prakash, S. G. and Park, C., "Shock Tube Spectroscopy of $C_3 + C_2H$ Mixture in the 140-700 mm Range," AIAA Paper 79-0094, Jan. 1979.

[20]Shinn, J. L., "Optical Absorption of Carbon and Hydrocarbon Species from Shock Heated Acetylene and Methane in the 135-200 nm Wavelength Range," *Progress in Astronautics and Aeronautics, Thermophysics of Atmospheric Entry*, edited by T. E. Horton, Vol. 82, AIAA, New York, 1982, pp. 68-80.

[21]Moss, J. N. and Simmonds, A. L., "Galileo Probe Forebody Flowfield Prediction During Jupiter Entry," AIAA Paper 82-0874, Mo., June 1982.

[22]Reda, D. C., "Comparative Transition Performance of Several Nosetip Materials as Defined by Ballistic-Range Testing," *Instrument Society of American Transactions*, Vol. 19, No. 1, Jan.-March 1980, pp. 83-98.

[23]Reda, D. C., "Correlation of Nosetip Boundary-Layer Transition Data Measured in Ballistic-Range Experiments," *AIAA Journal*, Vol. 19, No. 3, March 1981, pp. 329-339.

[24]Park, C., "Injection-Induced Turbulence in Stagnation-Point Boundary Layers," *AIAA Journal*, Vol. 22, Feb. 1984, pp. 219-225.

[25]Schlichting, H., *Boundary Layer Theory*, McGraw-Hill Book Co., New York, 1960, pp. 534-565.